The Astrophysical Journal, 949:117 (6pp), 2023 June 1 https://doi.org/10.3847/1538-4357/acc8d7

Search for Gravitational Waves from Scorpius X-1 in LIGO O3 Data with Corrected Orbital Ephemeris

John T. Whelan[1], Rodrigo Tenorio[2], Jared K. Wofford[3], James A. Clark[4], Edward J. Daw[5], Evan Goetz[6], David Keitel[2], Ansel Neunzert[7], Alicia M. Sintes[2], Katelyn J. Wagner[3], Graham Woan[8], Thomas L. Killestein[9], and Danny Steeghs[9,10]

[1] School of Mathematical Sciences and Center for Computational Relativity and Gravitation, Rochester Institute of Technology, Rochester, NY 14623, USA
john.whelan@ligo.org
[2] Departament de Física, Institut d'Aplicacions Computacionals i de Codi Comunitari (IAC3), Universitat de les Illes Balears, and Institut d'Estudis Espacials de Catalunya (IEEC), Carretera de Valldemossa km 7.5, E-07122 Palma, Spain
[3] School of Physics and Astronomy and Center for Computational Relativity and Gravitation, Rochester Institute of Technology, Rochester, NY 14623, USA
[4] LIGO Laboratory, California Institute of Technology, Pasadena, CA 91125, USA
[5] The University of Sheffield, Sheffield S10 2TN, UK
[6] University of British Columbia, Vancouver, BC V6T 1Z4, Canada
[7] LIGO Hanford Observatory, Richland, WA 99352, USA
[8] SUPA, University of Glasgow, Glasgow G12 8QQ, UK
[9] Department of Physics, University of Warwick, Gibbet Hill Road, Coventry CV4 7AL, UK
[10] OzGRav-Monash, School of Physics and Astronomy, Monash University, VIC 3800, Australia
Received 2023 February 20; revised 2023 March 24; accepted 2023 March 28; published 2023 June 5

Abstract

Improved observational constraints on the orbital parameters of the low-mass X-ray binary Scorpius X-1 were recently published in Killestein et al. In the process, errors were corrected in previous orbital ephemerides, which have been used in searches for continuous gravitational waves from Sco X-1 using data from the Advanced LIGO detectors. We present the results of a reanalysis of LIGO detector data from the third observing run of Advanced LIGO and Advanced Virgo using a model-based cross-correlation search. The corrected region of parameter space, which was not covered by previous searches, was about 1/3 as large as the region searched in the original O3 analysis, reducing the required computing time. We have confirmed that no detectable signal is present over a range of gravitational-wave frequencies from 25 to 1600 Hz, analogous to the null result of Abbott et al. Our search sensitivity is comparable to that of Abbott et al., who set upper limits corresponding, between 100 and 200 Hz, to an amplitude h_0 of about 10^{-25} when marginalized isotropically over the unknown inclination angle of the neutron star's rotation axis, or less than 4×10^{-26} assuming the optimal orientation.

Unified Astronomy Thesaurus concepts: Gravitational wave astronomy (675); Gravitational waves (678); Low-mass x-ray binary stars (939); Neutron stars (1108)

1. Introduction

The low-mass X-ray binary (LMXB) Scorpius X-1 (ScoX1), which is presumed to consist of a neutron star (NS) of mass $\approx 1.4 M_\odot$ in a binary orbit with a companion star of mass $\approx 0.4 M_\odot$ (Steeghs & Casares 2002), is a very promising potential source of continuous gravitational waves (GWs), generated by the spin of the NS (Bildsten 1998; Watts et al. 2008). As such, it has been the target of a number of searches (Abbott et al. 2007, 2017a, 2017b, 2017c, 2019a, 2019b, 2021, 2022b, 2022a; Aasi et al. 2015a; Meadors et al. 2017; Zhang et al. 2021) using data from the Advanced LIGO GW detectors (Aasi et al. 2015b), which have conducted three observing runs (O1, O2, and O3), the last two in coordination with Advanced Virgo (Acernese et al. 2015). As the spin frequency of ScoX1 is unknown, searches typically cover a wide range of the intrinsic GW signal frequency f_0, which in the simplest model is twice the spin frequency. Some of these searches, notably the cross-correlation method (Dhurandhar et al. 2008; Whelan et al. 2015) and the Viterbi method (Suvorova et al. 2016, 2017), are sensitive to aspects of the signal model, notably the parameters of the binary orbit. Hence, a campaign of electromagnetic observations and analyses known as "Precision Ephemerides for Gravitational-Wave Searches" (PEGS) has produced a series of updates to the orbital ephemeris for ScoX1 (Galloway et al. 2014; Wang et al. 2018; Killestein et al. 2023), which have been used to choose the parameter-space region covered in the GW searches. The most recent update, known as PEGS IV (Killestein et al. 2023), in addition to producing a more refined ephemeris also corrected errors in the previously published PEGS I (Galloway et al. 2014) and PEGS III (Wang et al. 2018) ephemerides.[11] This means that the parameter-space region searched by the analysis of O1 data in Abbott et al. (2017c), which used elements of PEGS I and PEGS III, as well as the O2 and O3 analyses in Abbott et al. (2019b, 2022b, 2022a), Zhang et al. (2021), which used PEGS III, did not overlap with the likely regions of parameter space according to the PEGS IV ephemeris, nor with the revised PEGS I and PEGS III ephemerides published in Killestein et al. (2023).[12] This paper presents a reanalysis of the LIGO O3 data (Abbott et al. 2023) according to the method

[11] PEGS II (Premachandra et al. 2016) was an ephemeris for Cygnus X-2 rather than ScoX1, and is not relevant to this work.
[12] The analysis of LIGO O1 data in Abbott et al. (2017b) used the orbital period from the PEGS I ephemeris, but because it used the method of Suvorova et al. (2016, 2017), which does not require the orbital phase, it was not affected in the same way as the other analyses.

of Abbott et al. (2022a), but with the parameter space determined by the PEGS IV ephemeris.

2. Orbital Ephemerides for Scorpius X-1

The signal model for GWs from an LMXB is a continuous signal with nearly constant intrinsic amplitude and frequency, Doppler-modulated by the relative motion of the source and the detector. As the Doppler modulation depends upon the extrinsic parameters of the system, including the sky position and orbital parameters of the binary system, accurate ranges of values for those parameters are an important input into GW searches. Since the sky location of ScoX1 is precisely known (Bradshaw et al. 1999; Abbott et al. 2007), and the orbital eccentricity is believed to be small (Steeghs & Casares 2002; Wang et al. 2018; Killestein et al. 2023), the important residual uncertainty is in the orbital velocity, period, and phase of the NS. The projected orbital velocity K_1 of the NS is usually described for GW searches in terms of the projected semimajor axis $a \sin i = K_1 P_{\rm orb}/(2\pi)$ of the orbit, measured in light-seconds.[13] Estimation of K_1 is particularly difficult for ScoX1 (Galloway et al. 2014), and the best constraint remains that of Wang et al. (2018), $40\,{\rm km\,s^{-1}} \lesssim K_1 \lesssim 90\,{\rm km\,s^{-1}}$. The orbital phase is generally described by the time at which the system reaches some reference point in its orbit. For GW searches, this is typically the time of ascension $t_{\rm asc}$, when the NS crosses the ascending node, moving away from the observer. This is one-quarter of a period before the other typically quoted reference time, of inferior conjunction of the companion star. Given a value of $t_{\rm asc}$ and $P_{\rm orb}$, an equivalent time of ascension in a later epoch $t_{\rm asc}' = t_{\rm asc} + n_{\rm orb} P_{\rm orb}$ can be obtained by adding an integer number $n_{\rm orb}$ of orbits (Whelan et al. 2015). For analysis of LIGO O3 data, it is convenient to choose a $t_{\rm asc}'$ value in the middle of the observing run, which lasted from 2019 April 1 to 2020 March 27, corresponding to GPS time 1,238,166,018 to 1,269,363,618.

The parameter-space ranges used for searches of O2 and O3 data (Abbott et al. 2019b, 2022b, 2022a; Zhang et al. 2021) were generated using the PEGS III ephemeris (Wang et al. 2018). Killestein et al. (2023) subsequently published the improved PEGS IV ephemeris, also documenting calibration errors in PEGS III. The values of $P_{\rm orb}$ and $t_{\rm asc}$ in these ephemerides are summarized in Table 1, which shows that the $t_{\rm asc}$ range originally published in Wang et al. (2018) is inconsistent with current estimates of that parameter. In Figure 1, we show the plausible ranges of $P_{\rm orb}$ and $t_{\rm asc}'$ (propagated to the middle of O3), along with the region of parameter space searched in the cross-correlation analysis (Abbott et al. 2022a), and in the reanalysis presented in this paper. We see that the parameter-space region searched in the original O3 search is inconsistent with the PEGS IV ephemeris, but the region searched in the present reanalysis has about 1/3 the area in parameter space, allowing a search to be performed more quickly at the same sensitivity.

3. Reanalysis of LIGO O3 Data with Cross-correlation Pipeline

We present here the results of a reanalysis of the LIGO O3 data (Abbott et al. 2023) using the cross-correlation search (Whelan et al. 2015), with the revised PEGS IV ephemeris of Killestein et al. (2023). Full details of the analysis pipeline are given in Abbott et al. (2022a). We highlight here changes made in light of the revised ephemeris.

The search was performed over a range of signal frequencies from 25 to 1600 Hz. Since the search is tunable, with the coherence time $T_{\rm max}$ chosen to balance computing cost and sensitivity, different $T_{\rm max}$ values are chosen across signal frequency and orbital parameter space to roughly optimize the chance of detecting a signal. The same coherence times were used as in Abbott et al. (2022a), with $240\,{\rm s} \leqslant T_{\rm max} \leqslant 18{,}720\,{\rm s}$. As in Abbott et al. (2022a), the search covered a range of projected semimajor axes $1.44\,{\rm lt-s} \leqslant a \sin i \leqslant 3.25\,{\rm lt-s}$.[14] The $t_{\rm asc}'$–$P_{\rm orb}$ space was covered using the sheared period coordinate of Wagner et al. (2022), which for the reanalysis was defined as

$$\tilde{P} = P_{\rm orb} - 2.47 \times 10^{-4}(t_{\rm asc}' - 1{,}255{,}015{,}866). \quad (1)$$

The range of $t_{\rm asc}'$ values was set to $1{,}255{,}015{,}866 \pm 3 \times 55$, while the $P_{\rm orb}$ values were constrained to lie in an ellipse centered on $(\tilde{P}, t_{\rm asc}') = (68{,}023.91\,{\rm s}, 1{,}255{,}015{,}866)$ with semiaxes of $3.3 \times 0.010\,{\rm s}$ for $\tilde{P}$ and $3.3 \times 55\,{\rm s}$ for $t_{\rm asc}'$. The boundaries of this region in $(P_{\rm orb}, t_{\rm asc}')$ space are shown in solid black lines in Figure 1. Note that the software bug that led to the slightly misaligned definition of $\tilde{P}$ used in Abbott et al. (2022a) was fixed before the reanalysis, so the search region now lines up with the PEGS IV prior uncertainty region, as seen in Figure 1. As in Abbott et al. (2022a), the $\tilde{P}$ coordinate was unresolved for most analysis jobs, and a single template was sufficient to cover the range $68{,}023.91 \pm 3.3 \times 0.010\,{\rm s}$.

As in Abbott et al. (2022a), the search was carried out at a nominal parameter-space mismatch of 0.25. Due to the reduced parameter ranges in the more precise PEGS IV ephemeris, this

Table 1
Orbital Parameters in the PEGS III and PEGS IV Ephemerides

Parameter	PEGS III[a]	PEGS IV[b]
$P_{\rm orb}$ (s)	$68{,}023.86 \pm 0.043$	$68{,}023.91 \pm 0.017$
$t_{\rm asc}$ (GPS s)[c]	$974{,}416{,}624 \pm 50$	$1{,}078{,}153{,}676 \pm 33$
$t_{\rm asc}'$ (GPS s)[d]	$1{,}255{,}015{,}049 \pm 185$	$1{,}255{,}015{,}866 \pm 55$
Corr($P_{\rm orb}$, $t_{\rm asc}'$)[e]	0.96	0.80

Notes. Uncertainties are 1σ.
[a] Values in this column are inferred from Wang et al. (2018).
[b] Values in this column are inferred from Killestein et al. (2023).
[c] The time of ascension $t_{\rm asc}$, at which the NS crosses the ascending node (moving away from the observer), measured in the solar system barycenter, is derived from the time of inferior conjunction of the companion by subtracting $P_{\rm orb}/4$. The values quoted in this row are those for which the correlations in the $P_{\rm orb}$ and $t_{\rm asc}$ uncertainties are negligible, and correspond to 2010 November 21 23:16:49 UTC and 2014 March 6 15:07:40 UTC, respectively.
[d] The time of ascension $t_{\rm asc}'$ after propagating $t_{\rm asc}$ forward by $n_{\rm orb}$ orbits (4125 and 2600, respectively), corresponding to times of 2019 October 13 15:17:11 UTC and 2019 October 13 15:30:48 UTC, near the middle of the O3 run. The uncertainty is obtained by combining the uncertainty in $t_{\rm asc}'$ in quadrature with $n_{\rm orb}$ times the uncertainty in $P_{\rm orb}$ (Whelan et al. 2015).
[e] The correlation between the uncertainties in $P_{\rm orb}$ and $t_{\rm asc}' = t_{\rm asc} + n_{\rm orb} P_{\rm orb}$, given uncorrelated uncertainties in $P_{\rm orb}$ and $t_{\rm asc}$.
References. Wang et al. (2018), Killestein et al. (2023).

[13] Since the fractional uncertainty on $P_{\rm orb}$ is much smaller than that in K_1, no significant correlation between $a \sin i$ and $P_{\rm orb}$ is introduced by this convention.

[14] There was a slight difference arising from converting the range $40 \leqslant K_1 \leqslant 90\,{\rm km\,s^{-1}}$ to $a \sin i$ using the revised period estimate, but well below the precision reported here.

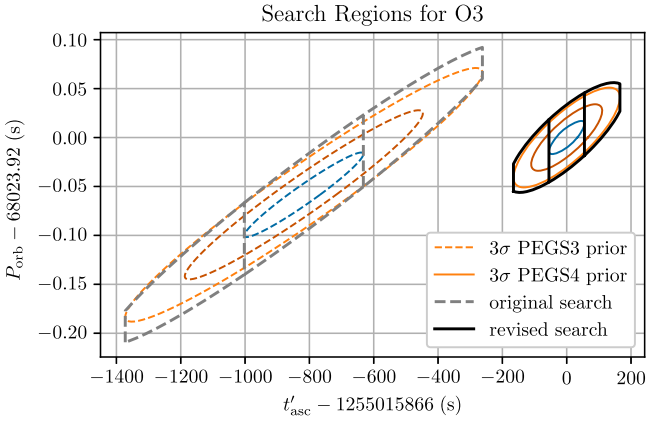

Figure 1. Prior uncertainties and search regions for O3 analyses. The dashed colored ellipses show curves of constant prior probability according to the PEGS III ephemeris of Wang et al. (2018), corresponding to 1σ, 2σ, and 3σ (containing 39.3%, 86.5%, and 98.9% of the prior probability, respectively). The solid colored ellipses show the same curves for the PEGS IV ephemeris of Killestein et al. (2023). The dashed gray lines show the search regions used in the O3 cross-correlation analysis of Abbott et al. (2022a); the central region, between the vertical lines, was searched with higher coherence times. The solid black lines show the search region for the present reanalysis.

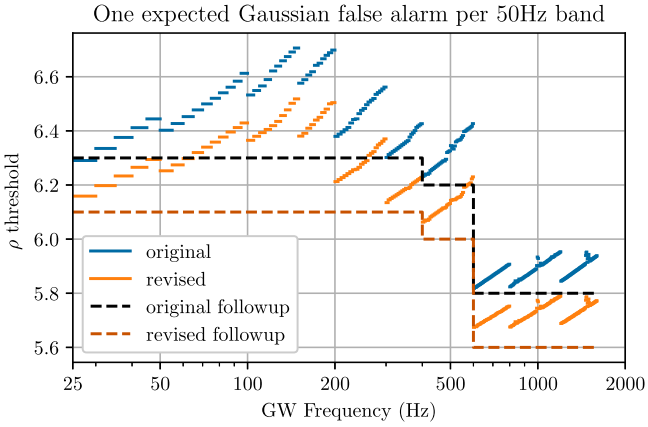

Figure 2. Selection of follow-up threshold as a function of GW frequency. If the data contained no signal and only Gaussian noise, each template in the parameter space would have some chance of producing a statistic value exceeding a given threshold. Within each 5 Hz frequency band, the total number of templates was computed and used to find the threshold at which the expected number of Gaussian outliers (assuming uncorrelated templates) above that value would be 0.1. The short blue lines show this quantity for the original O3 search in Abbott et al. (2022a); the short green lines show this for the present reanalysis. Because of the smaller parameter space searched with the PEGS IV ephemeris, the present search uses fewer templates (see Table 2), and therefore would be expected to have the specified number of false alarms at a lower threshold. We thus use a lower threshold for follow-ups in this analysis (dashed red line) than that in the original analysis (dashed black line.) Compare to Figure 4 of Abbott et al. (2022a).

required fewer templates than in the original analysis. As a consequence, the threshold for follow-up, which is set using the expected number of false alarms from Gaussian noise at a particular frequency, could be reduced, as shown in Figure 2. In the present search, we followed up candidates with a signal-to-noise ratio (S/N) above 6.1 from $25\,\mathrm{Hz} < f_0 < 400\,\mathrm{Hz}$, 6.0 for $400\,\mathrm{Hz} < f_0 < 600\,\mathrm{Hz}$, and 5.6 for $600\,\mathrm{Hz} < f_0 < 1600\,\mathrm{Hz}$, compared to 6.3, 6.2, and 5.8, respectively, in the original analysis of Abbott et al. (2022a).

The detection candidates that exceeded the follow-up threshold were subjected to a hierarchical follow-up using successively finer grids and longer coherence times. At each stage, the candidates for which the S/N from a search using only one detector (LIGO Hanford Observatory, hereafter LHO; or LIGO Livingston Observatory, hereafter LLO) exceeded the S/N obtained from the full data and were rejected as likely narrowband instrumental features (*lines*). The initial results were known as *level (0)*; *level (1)* used the same coherence time $T_{\rm max}$ and only refined the grid, while *level (2)* and *level (3)* each successively quadrupled $T_{\rm max}$ relative to the previous level, which would ideally double the S/N of a signal. If a candidate's S/N went down from one level of follow-up to the next, it was discarded. Table 2 shows the numbers of candidates surviving each level of follow-up. A total of 24 candidates survived level (3) of follow-up. For each of the candidates surviving level (2) (so that level (3) follow-up was run), Figure 3 shows the ratios of S/Ns at successive levels.

For the most part, we reproduce the results of Abbott et al. (2022a), that the outliers of the search do not increase their S/N upon follow-up in the way that simulated signals do. There is one possible exception: a candidate at a frequency of 510.71 Hz, which has S/N ρ of 6.08 at level (0), 6.48 at level (1), 9.58 at level (2), and 10.41 at level (3). Note that, while this candidate would not have made the follow-up threshold in the original search, which was 6.2 for frequencies between 400 and 600 Hz (as compared with 6.0 in the follow-up), there is no such outlier in the original search with the PEGS III ephemeris; all of the templates searched with $510.70\,\mathrm{Hz} < f_0 < 510.72\,\mathrm{Hz}$ produced S/N $\rho < 4.5$ in the original search.

We have strong reasons to believe the outlier in the reanalysis is an instrumental artifact. The outlier is located in a frequency range heavily contaminated by violin modes in both LIGO detectors (Davis et al. 2021). The cross-correlation analysis excludes data at frequencies contaminated by known lines (Goetz et al. 2021) from the analysis. For LIGO Hanford Observatory (LHO), this includes data from 510.71527 to 510.72653 Hz, and for LLO, this includes data from 507.89972 to 516.25972 Hz. The relative amplitude of possible Doppler modulation for ScoX1 is $\lesssim 4 \times 10^{-4}$, so a signal with intrinsic frequency 510.7 Hz could be received at the detector with a frequency from ∼510.5 to ∼510.9 Hz. Thus LLO is completely excluded from the analysis of this candidate, as indicated by the blue *single detector* square in Figure 3. As a consequence, the S/N using only LHO data is the same as the S/N from the full search, and the *unknown line* veto cannot be applied to this candidate.

As an additional investigation, we reran the follow-up with no data excluded. The S/N of the candidate dropped to 4.95, while the S/N using only LHO increased to 65.90. (The S/N using only LLO was 2.45.) I.e., without the *known line* veto to eliminate LLO data, the outlier would have been eliminated as a possible candidate by the *unknown line* veto.

This outlier was further scrutinized by a multistage Markov Chain Monte Carlo follow-up using the method described in Tenorio et al. (2021) with the PyFstat package (Ashton & Prix 2018; Keitel et al. 2021; Ashton et al. 2022). The setup was identical to that of Abbott et al. (2022a): Templates were placed adaptively around the outlier to compute the semicoherent $\mathcal{F}$-statistic (Jaranowski et al. 1998; Cutler & Schutz 2005) using a decreasing number of coherent segments (660, 330, 92, 24, 4, and 1), which correspond to a coherence time ranging from half a day to the full observing run. A Bayes factor was computed using the $\mathcal{F}$-statistic values of consecutive stages corresponding to the loudest template. The signal

Table 2
Summary of Numbers of Templates and Candidates

f_0(Hz)		T_{max}(s)		ρ	Number of Templates	Expected Gauss. False Alarms[b]	Follow-up Level			
Min	Max	Min	Max	Thresh[a]			0[c]	1[d]	2[e]	3[f]
25	50	10,080	18,720	6.1	2.24×10^9	1.2	62	34	5	0
50	100	8160	14,280	6.1	9.65×10^9	5.1	134	115	41	0
100	150	6720	10,920	6.1	1.71×10^{10}	9.1	148	146	81	3
150	200	5040	8640	6.1	1.79×10^{10}	9.5	151	151	74	1
200	300	2400	4800	6.1	1.30×10^{10}	6.9	60	60	22	8
300	400	1530	3060	6.1	6.51×10^9	3.5	24	24	5	3
400	600	720	2160	6.0	9.96×10^9	9.8	312	199	20	9
600	800	360	360	5.6	7.34×10^8	7.9	8	8	0	0
800	1200	300	300	5.6	1.69×10^9	18.2	234	65	2	0
1200	1600	240	240	5.6	1.65×10^9	17.7	328	61	7	0

Notes. For each range of GW frequencies, this table shows the minimum and maximum coherence time T_{max} used for the search, the threshold in the S/N ρ used for follow-up, the total number of templates, and the number of candidates at various stages of the process. Compare to Table 3 of Abbott et al. (2022a).
[a] This is the threshold for initiating follow-up, i.e., to produce a level (0) candidate.
[b] This is the number of candidates that would be expected in Gaussian noise, given the number of templates and the follow-up threshold.
[c] This is the actual number of candidates (after clustering), which crossed the S/N threshold and were followed up.
[d] This is the number of candidates remaining after refinement. All of the candidates *missing* at this stage have been removed by the single-detector veto for unknown lines.
[e] This is the number of candidates remaining after each has been followed up with a T_{max} equal to 4 × the original T_{max} for that candidate. (True signals should approximately double their S/N; any candidates whose S/N goes down have been dropped.) All of the signals present at this stage are shown in Figure 3, which also shows the behavior of the search on simulated signals injected in software.
[f] This is the number of candidates remaining after T_{max} has been increased to 16 × its original value.

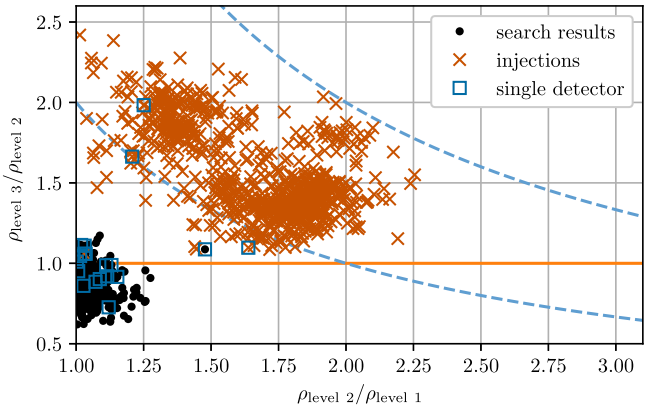

Figure 3. Ratios of follow-up statistics for search candidates and simulated signals. This plot shows all of the candidates that survived level (2) of follow-up (see Table 2). It shows the ratios of the S/N ρ after follow-up level (1) (at the original coherence time T_{max}), level (2) (at 4 × the original coherence time), and level (3) (at 16 × the original coherence time). For comparison, the results of the original injection analysis from Abbott et al. (2022a) are shown. The dashed lines are at constant values of $\rho_{level\ 3}/\rho_{level\ 1}$ equal to 2 and 4. Points below the solid line have $\rho_{level\ 3} < \rho_{level\ 2}$ and are therefore vetoed at follow-up level (2). The boxes labeled "single detector" are outliers or injections at GW frequencies where only one detector's data was included in the analysis because of known instrumental artifacts in the other detector. Compared to Figure 5 of Abbott et al. (2022a), we see one candidate (with $(\frac{\rho_{level\ 2}}{\rho_{level\ 1}}, \frac{\rho_{level\ 3}}{\rho_{level\ 2}}) \approx (1.48, 1.09)$), which increases its S/N marginally similarly to the least significant of the injections. As discussed in the text, this is a *single detector* outlier where only LHO data have been used, and it appears to be an instrumental artifact.

hypothesis assesses the consistency of these values, while comparing against the noise hypothesis checks the inconsistency of the final value with the background distribution. The resulting Bayes factor is significantly lower than expected for a signal detectable by this search. Moreover, the semicoherent $\mathcal{F}$-statistic accumulation of the outlier in the LHO data suggests an instrumental origin.

4. Conclusions and Outlook

We have reanalyzed the LIGO O3 data with the cross-correlation pipeline, using the corrected and improved PEGS IV ephemeris of Killestein et al. (2023). Having found no credible detection candidates, we reproduce the null result of Abbott et al. (2022a), that there is no GW signal from ScoX1 detectable at the level of sensitivity of that search. We do not produce an upper limit from the reanalysis, but as approximate sensitivity computations for the two searches agree, we conclude that the upper limits published in Abbott et al. (2022a) remain valid.

Since the cross-correlation analysis of this paper, as in Abbott et al. (2022a), does not explicitly consider a signal with stochastically varying frequency ("spin wandering")—although it is somewhat robust to it (Whelan et al. 2015)—there is information to be gained from reanalysis of the O3 data using a hidden Markov model as in Abbott et al. (2022b).

The O4 run of Advanced LIGO, Advanced Virgo, and KAGRA (Akutsu et al. 2021) is scheduled to begin in May 2024 and run for approximately 18 months (LIGO-Virgo-KAGRA Collaboration 2023). The improved sensitivity of the detectors will enable more sensitive searches for GWs from ScoX1, and the greater precision of the PEGS IV ephemeris will enable the search to be done more efficiently.

We wish to thank the members of the LIGO-Virgo-KAGRA Collaboration continuous waves group for useful feedback. J.T.W., J.K.W., and K.J.W. were supported by NSF grants PHY-1806824 and PHY-2110460. J.T.W. and J.K.W. thank Goethe University Frankfurt. R.T., D.K., and A.M.S. are supported by the Spanish Ministerio de Ciencia e Innovación and the Spanish Agencia Estatal de Investigación grant PID2019-106416GB-I00/AEI/MCIN/10.13039/501100011033, European Union NextGenerationEU funds (PRTR-C17.I1), the Comunitat Autònoma de les Illes Balears through the Direcció General de Política Universitaria i Recerca with funds from the

Tourist Stay Tax Law 2017-006 (PRD2018/24, PDR2020/11), the Conselleria de Fons Europeus, Universitat i Cultura del Govern de les Illes Balears, the FEDER Operational Program 2021–2027 of the Balearic Islands, and EU COST Actions CA18108 and CA17137. R.T. is supported by the Spanish Ministerio de Universidades (ref. FPU 18/00694). J.C. was supported by NSF grant PHY-1764464. E.G. is grateful for the support of the John Edwards Leadership Fund. D.K. is supported by the Spanish Ministerio de Ciencia, Innovación y Universidades (ref. BEAGAL 18/00148), cofinanced by the Universitat de les Illes Balears and grants RED2022-134204-E and RED2022-134411-T. T.L.K. is supported by the UK Science and Technology Facilities Council (STFC), grant No. ST/T506503/1. A.N. was supported by NSF awards PHY-1912598 and PHY-1944412 and thanks the University of Washington, Bothell. D.S. is supported by STFC, grant Nos. ST/T007184/1, ST/T003103/1, and ST/T000406/1.

The authors are grateful for computational resources provided by LIGO Laboratory, supported by National Science Foundation grants PHY-1626190 and PHY-1700765, by the Open Science Grid (OSG) Consortium (Pordes et al. 2007; Sfiligoi et al. 2009; OSG 2006), which is supported by the National Science Foundation awards #2030508 and #1836650, and by the Digital Research Alliance of Canada.[15] Scripts and data pertaining to the original O3 analysis are available at https://dcc.ligo.org/LIGO-T2200419/public.

The analysis reported in this paper also used the segment lists of Goetz & Riles (2023) and the self-gating procedure documented in Zweizig & Riles (2021).

This research has made use of data available from the Gravitational Wave Open Science Center,[16] a service of LIGO Laboratory, the LIGO Scientific Collaboration, the Virgo Collaboration, and KAGRA. LIGO Laboratory and Advanced LIGO are funded by the United States National Science Foundation (NSF) as well as the Science and Technology Facilities Council (STFC) of the United Kingdom, the Max-Planck-Society (MPS), and the State of Niedersachsen/Germany for support of the construction of Advanced LIGO and construction and operation of the GEO600 detector. Additional support for Advanced LIGO was provided by the Australian Research Council. Virgo is funded, through the European Gravitational Observatory (EGO), by the French Centre National de Recherche Scientifique (CNRS), the Italian Istituto Nazionale di Fisica Nucleare (INFN), and the Dutch Nikhef, with contributions by institutions from Belgium, Germany, Greece, Hungary, Ireland, Japan, Monaco, Poland, Portugal, Spain. KAGRA is supported by Ministry of Education, Culture, Sports, Science and Technology (MEXT), Japan Society for the Promotion of Science (JSPS) in Japan; National Research Foundation (NRF) and Ministry of Science and ICT (MSIT) in Korea; Academia Sinica (AS) and National Science and Technology Council (NSTC) in Taiwan.

Software: `LALSuite` (LIGO Scientific Collaboration 2018), `LatticeTiling` (Wette 2014), `PyFstat` (Ashton & Prix 2018; Keitel et al. 2021; Ashton et al. 2022), `ptemcee` (Foreman-Mackey et al. 2013; Vousden et al. 2016), `numpy` (Harris et al. 2020), `matplotlib` (Hunter 2007), `scipy` (Virtanen et al. 2020), `SwigLAL` (Wette 2020).

This paper has been assigned LIGO document No. LIGO-P2300042-v8.

[15] https://alliancecan.ca
[16] http://gwosc.org

ORCID iDs

John T. Whelan https://orcid.org/0000-0001-5710-6576
Rodrigo Tenorio https://orcid.org/0000-0002-3582-2587
Jared K. Wofford https://orcid.org/0000-0002-4301-2859
James A. Clark https://orcid.org/0000-0003-3243-1393
Edward J. Daw https://orcid.org/0000-0002-3780-5430
Evan Goetz https://orcid.org/0000-0003-2666-721X
David Keitel https://orcid.org/0000-0002-2824-626X
Ansel Neunzert https://orcid.org/0000-0003-0323-0111
Alicia M. Sintes https://orcid.org/0000-0001-9050-7515
Katelyn J. Wagner https://orcid.org/0000-0002-7255-4251
Graham Woan https://orcid.org/0000-0003-0381-0394
Thomas L. Killestein https://orcid.org/0000-0002-0440-9597
Danny Steeghs https://orcid.org/0000-0003-0771-4746

References

Aasi, J., Abbott, B. P., Abbott, R., et al. 2015a, PhRvD, 91, 062008
Aasi, J., Abbott, B. P., Abbott, R., et al. 2015b, cqg, 32, 074001
Abbott, B., Abbott, R., Adhikari, R., et al. 2007, PhRvD, 76, 082001
Abbott, B. P., Abbott, R., Abbott, T. D., et al. 2017a, PhRvL, 118, 121102
Abbott, B. P., Abbott, R., Abbott, T. D., et al. 2017b, PhRvD, 95, 122003
Abbott, B. P., Abbott, R., Abbott, T. D., et al. 2017c, ApJ, 847, 47
Abbott, B. P., Abbott, R., Abbott, T. D., et al. 2019a, PhRvD, 100, 062001
Abbott, B. P., Abbott, R., Abbott, T. D., et al. 2019b, PhRvD, 100, 122002
Abbott, B. P., Abbott, T. D., Abraham, S., et al. 2021, PhRvD, 104, 022005
Abbott, B. P., Abe, H., Acernese, F., et al. 2022a, ApJL, 941, L30
Abbott, B. P., Abe, H., Acernese, F., et al. 2022b, PhRvD, 106, 062002
Abbott, R., Abe, H., Acernese, F., et al. 2023, arXiv:2302.03676
Acernese, F., Agathos, M., Agatsuma, K., et al. 2015, cqg, 32, 024001
Akutsu, T., Ando, M., Arai, K., et al. 2021, PTEP, 2021, 05A102
Ashton, G., Keitel, D., Prix, R., & Tenorio, R. 2022, yFstat: v1.19.1, Zenodo, doi:10.5281/zenodo.7458002
Ashton, G., & Prix, R. 2018, PhRvD, 97, 103020
Bildsten, L. 1998, ApJL, 501, L89
Bradshaw, C. F., Fomalont, E. B., & Geldzahler, B. J. 1999, ApJL, 512, L121
Cutler, C., & Schutz, B. F. 2005, PhRvD, 72, 063006
Davis, D., Areeda, J. S., Berger, B. K., et al. 2021, cqg, 38, 135014
Dhurandhar, S., Krishnan, B., Mukhopadhyay, H., & Whelan, J. T. 2008, PhRvD, 77, 082001
Foreman-Mackey, D., Hogg, D. W., Lang, D., & Goodman, J. 2013, PASP, 125, 306
Galloway, D. K., Premachandra, S., Steeghs, D., et al. 2014, ApJ, 781, 14
Goetz, E., Neunzert, A., Riles, K., et al. 2021, O3 lines and combs in found in self-gated C01 data, LIGO Document T2100200-v2, T2100200-v2 LIGO, https://dcc.ligo.org/LIGO-T2100200/public
Goetz, E., & Riles, K. 2023, Segments used for creating standard SFTs in O3 data, LIGO Document T2300068-v2, T-2300068-v2 LIGO, https://dcc.ligo.org/LIGO-T2300068/public
Harris, C. R., Millman, K. J., van der Walt, S. J., et al. 2020, Natur, 585, 357
Hunter, J. D. 2007, CSE, 9, 90
Jaranowski, P., Krolak, A., & Schutz, B. F. 1998, PhRvD, 58, 063001
Keitel, D., Tenorio, R., Ashton, G., & Prix, R. 2021, JOSS, 6, 3000
Killestein, T. L., Mould, M., Steeghs, D., Galloway, D. K., et al. 2023, MNRAS, 520, 5317
LIGO-Virgo-KAGRA Collaboration 2018, LIGO Algorithm Library—LALSuite, free software (GPL), doi:10.7935/GT1W-FZ16
LIGO-Virgo-KAGRA Collaboration 2023, LIGO, Virgo and KAGRA Observing Run Plans 19 January 2023 Update, https://observing.docs.ligo.org/plan/
Meadors, G. D., Goetz, E., Riles, K., Creighton, T., & Robinet, F. 2017, PhRvD, 95, 042005
OSG 2006, OSPool, computing resource, doi:10.21231/906P-4D78
Pordes, R., Petravick, D., Kramer, B., et al. 2007, JPhCS, 78, 012057
Premachandra, S. S., Galloway, D. K., Casares, J., Steeghs, D. T., & Marsh, T. R. 2016, ApJ, 823, 106

Sfiligoi, I., Bradley, D. C., Holzman, B., et al. 2009, in 2009 WRI World Congress on Computer Science and Information Engineering, The Pilot Way to Grid Resources Using glideinWMS (Piscataway, NJ: IEEE), 428
Steeghs, D., & Casares, J. 2002, ApJ, 568, 273
Suvorova, S., Clearwater, P., Melatos, A., et al. 2017, PhRvD, 96, 102006
Suvorova, S., Sun, L., Melatos, A., Moran, W., & Evans, R. 2016, PhRvD, 93, 123009
Tenorio, R., Keitel, D., & Sintes, A. M. 2021, PhRvD, 104, 084012
Virtanen, P., Gommers, R., Oliphant, T. E., et al. 2020, NatMe, 17, 261
Vousden, W. D., Farr, W. M., & Mandel, I. 2016, MNRAS, 455, 1919
Wagner, K. J., Whelan, J. T., Wofford, J. K., & Wette, K. 2022, cqg, 39, 075013
Wang, L., Steeghs, D., Galloway, D. K., Marsh, T., & Casares, J. 2018, MNRAS, 478, 5174
Watts, A. L., Krishnan, B., Bildsten, L., & Schutz, B. F. 2008, MNRAS, 389, 839
Wette, K. 2014, PhRvD, 90, 122010
Wette, K. 2020, SoftX, 12, 100634
Whelan, J. T., Sundaresan, S., Zhang, Y., & Peiris, P. 2015, PhRvD, 91, 102005
Zhang, Y., Papa, M. A., Krishnan, B., & Watts, A. L. 2021, ApJL, 906, L14
Zweizig, J., & Riles, K. 2021, Information on self-gating of h(t) used in O3 continuous-wave and stochastic searches, LIGO Document T2000384-v4, T2000384-v4 LIGO, https://dcc.ligo.org/LIGO-T2000384/public